Geochemical Perspectives Letters

Stable vanadium isotopes as a redox proxy in magmatic systems?

J. Prytulak[1*], P.A. Sossi[2], A.N. Halliday[3], T. Plank[4], P.S. Savage[5], J.D. Woodhead[6]

Abstract

Recycling pathways of multivalent elements, that impact our understanding of diverse geological processes from ore formation to the rise of atmospheric oxygen, depend critically on the spatial and temporal variation of oxygen fugacity (fO_2) in the Earth's interior. Despite its importance, there is currently no consensus on the relative fO_2 of the mantle source of mid-ocean ridge basalts compared to the sub-arc mantle, regions central to the mediation of crust-mantle mass balances. Here we present the first stable vanadium isotope measurements of arc lavas, complemented by non-arc lavas and two co-genetic suites of fractionating magmas, to explore the potential of V isotopes as a redox proxy. Vanadium isotopic compositions of arc and non-arc magmas with similar MgO overlap with one another. However, V isotopes display strikingly large, systematic variations of ~2‰ during magmatic differentiation in both arc and non-arc settings. Calculated bulk V Rayleigh fractionation factors (1000 $\ln\alpha_{min\text{-}melt}$ of -0.4 to -0.5‰) are similar regardless of the oxidation state of the evolving magmatic system, which implies that V isotope fractionation is most influenced by differences in bonding environment between minerals and melt rather than changes in redox conditions. Thus, although subtle fO_2 effects may be present, V isotopes are not a direct proxy for oxygen fugacity in magmatic systems.

Received 29 July 2016 | Accepted 3 October 2016 | Published 26 October 2016

Introduction

Oxygen fugacity (fO_2), the chemical potential of oxygen, varies over ten orders of magnitude in igneous systems (Carmichael, 1991). Knowledge of mantle fO_2 is of critical importance for understanding the speciation of fluids in subduction zones and thus the efficiency of elemental transfer from slab to surface. Oxygen

1. Department of Earth Science and Engineering, Imperial College London, UK
* Corresponding author (email: j.prytulak@imperial.ac.uk)
2. Institut de Physique du Globe de Paris, France
3. Department of Earth Science, University of Oxford, UK
4. Lamont-Doherty Earth Observatory, Columbia University, USA
5. Department of Earth and Environmental Sciences, University of St. Andrews, UK
6. School of Earth Sciences, University of Melbourne, Australia

fugacity is often reported in log units relative to a buffer reaction, commonly fayalite-magnetite-quartz (FMQ). Early study of mantle fO_2 employed oxygen thermobarometry, proposing that subduction zone magmas and their sources are more oxidised (>FMQ +1) than those found at mid-ocean ridges (~FMQ) (*e.g.*, see review of Frost and McCammon, 2008).

However, the association of mantle fO_2 with tectonic setting has become contested following the introduction of novel approaches to its determination. The development of new proxies based on ratios of redox to non-redox sensitive elements, such as V/Sc and Fe/Zn, coupled with synthesis of global chemical databases such as GEOROC (http://georoc.mpch-mainz.gwdg.de/georoc/) and PETDB (http://www.earthchem.org/petdb), has led to the counterintuitive proposal that there is no difference in fO_2 between the *mantle sources* of arc and MORB lavas (Lee *et al.*, 2005, 2010). Despite this hypothesis, there is a consensus that basaltic melts found in arcs are more oxidised than their MORB counterparts, given, for example, their elevated $Fe^{3+}/\sum Fe$ ratios measured in melt inclusions (*e.g.*, Kelley and Cottrell, 2009). In order to explain how oxidised arc basalts and more reduced MORBs can be derived from sources with similar fO_2, processes subsequent to magma generation such as degassing and crystal fractionation have been invoked (*e.g.*, Mallmann and O'Neill, 2009; Lee *et al.*, 2010). Evidence gleaned from both experimental and natural suites is conflicting, with cases of $Fe^{3+}/\sum Fe$ increasing, decreasing and remaining invariant during magmatic degassing and crystallisation (*e.g.*, Brounce *et al.*, 2014; Waters and Lange, 2016). Thus lingering uncertainty as to whether the elevated $Fe^{3+}/\sum Fe$ in arc lavas is derived from their sources or during differentiation fuels continued debate.

The stable isotope composition of multivalent elements is theoretically linked to fO_2. High temperature fractionation of stable isotopes is dictated by the vibrational frequencies of chemical bonds, with higher frequencies having larger bond force constants (K) and preferring heavier isotopes. An instructive estimate of the force constant is given by the mean bond strength: the quotient of average valence and co-ordination number (Pauling, 1929). Thus, atoms associated with higher oxidation state and/or lower co-ordination should, on average, incorporate a greater proportion of heavier isotopes. Therefore the possibility of resolving transition metal stable isotope variations in high temperature settings has the potential to define mantle fO_2 more clearly. Although it is tempting to employ simple comparative geochemistry (*i.e.* heavier isotope compositions equate to more oxidising conditions), the interplay between co-ordination environment and valence state is vital to interpreting the effect of changing fO_2 on isotope fractionation.

Vanadium as a Redox Proxy

Vanadium is a moderately incompatible, refractory multivalent (2+, 3+, 4+, 5+) element and the strong dependence of its partitioning behaviour on fO_2 is well-established (*e.g.*, Canil, 1997; Toplis and Corgne, 2002; Mallmann and O'Neill, 2009). In all major mantle phases, vanadium becomes more incompatible with

increasing fO_2, leading to the application of V as a redox proxy (*e.g.*, Shervais, 1982; Canil, 1997; Lee *et al.*, 2005; Mallmann and O'Neill, 2009). However, using concentrations alone results in fO_2 uncertainties on the order of 1-2 log units due to variations in degree of melting, original source concentration, and fractionating mineral assemblages (Lee *et al.*, 2003).

Vanadium has two stable isotopes, ^{51}V and ^{50}V. Their ratio is reported as per mille deviations, $\delta^{51}V$, relative to the AA (Alfa Aesar) V solution standard, defined as 0 ‰ (see Nielsen *et al.*, 2011). The extreme natural $^{51}V/^{50}V$ ratio of ~420 coupled with isobaric interferences from ^{50}Cr and ^{50}Ti on the minor ^{50}V isotope have historically prevented analyses to a precision useful for high temperature applications. These obstacles were recently overcome, and the first analytical protocol to determine $\delta^{51}V$ to a precision better than ±0.15 ‰ 2sd (Nielsen *et al.*, 2011; Prytulak *et al.*, 2011) demonstrated resolvable variations in igneous rocks of different silica content ($\delta^{51}V_{basalts} < \delta^{51}V_{andesites}$). We present the first $\delta^{51}V$ measurements directly exploring the potential of $\delta^{51}V$ as a redox proxy in magmatic systems. Specifically, we investigate the effect of magmatic evolution and determine if a resolvable $\delta^{51}V$ difference exists between arc and non-arc lavas.

Methods

The oxygen fugacity of the two tectonic settings investigated herein (Mariana arc and Hekla, Iceland) have been previously determined by two independent means: by way of Fe^{3+}/Fe^{2+} ratios that are converted to fO_2, and by Fe-Ti oxybarometry. Both methods indicate that Mariana arc basalts are generally ~1-2 log units more oxidised compared to Icelandic basalts from Hekla (*e.g.*, de Moor *et al.*, 2005; Moune *et al.*, 2007; Brounce *et al.*, 2014; Shorttle *et al.*, 2015). We chose forty whole rock samples from three well-studied lava suites: 1) primitive arc lavas of the Mariana Central Island Province (CIP; Elliott *et al.*, 1997), 2) co-genetic lavas from Anatahan volcano in the Mariana arc (Wade *et al.*, 2005) and 3) co-genetic lavas from Hekla volcano, Iceland (Savage *et al.*, 2011). Published major, trace and isotopic data are found in Table S-1.

Chemical separation and V isotope measurements were made at Oxford University and Imperial College London, following Nielsen *et al.* (2011). Description of methods and isotopic data are found in the Supplementary Information and Table S-2.

Results and Discussion

Two key observations arise from Figure 1. First, there is a striking range of ~2 ‰ towards heavy $\delta^{51}V$ with progressive differentiation in both suites of lavas, which is an order of magnitude larger than Fe isotope variations in fractionating magmas (*e.g.*, Schuessler *et al.*, 2009; Sossi *et al.*, 2012). Second, basaltic lavas from the Marianas, Iceland and MORB have overlapping $\delta^{51}V$.

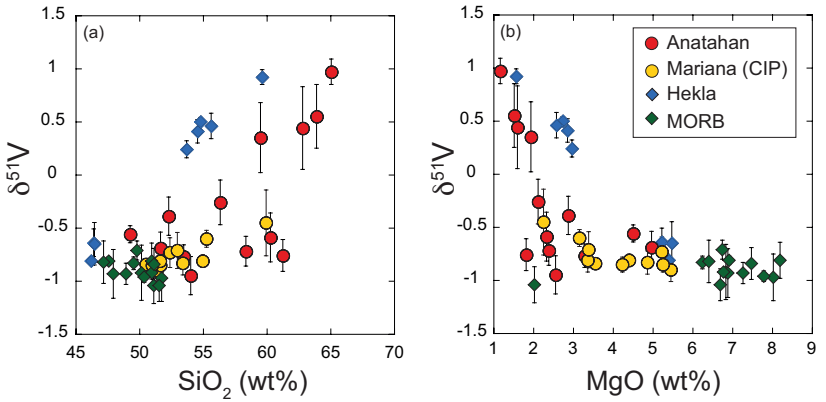

Figure 1 $\delta^{51}V$ variations with SiO_2 **(a)** and MgO **(b)**. CIP = Central Island Province. MORB data from Prytulak *et al.* (2013). Uncertainties on isotope measurements are external 2 sd.

The remarkable magnitude of high temperature $\delta^{51}V$ fractionation towards heavy values with magmatic evolution is unlikely to be due to the difference in calculated fO_2 between Hekla and the Marianas, because the $\delta^{51}V$ variation is similar for both suites. Instead, the primary control on isotope fractionation appears to be differences in mineral-melt bonding environment. Oxide minerals such as (titano)magnetite host the majority of V in magmatic systems. Trivalent vanadium is preferentially incorporated in the VI-fold sites of (titano)magnetite, the thermodynamically stable configuration (O'Neill and Navrotsky, 1984) resulting from its high octahedral site preference energy. Vanadium's oxidation and co-ordination in silicate melts is not constrained by stoichiometry, but is always higher and lower, respectively, than in co-existing (titano)magnetite (Righter *et al.*, 2006). Thus (titano)magnetite (and other ferromagnesian minerals) should be isotopically light, and crystallisation will lead to a progressively heavier residual melt. A significant departure to heavy $\delta^{51}V$ is observed at ~60 wt. % SiO_2 at Anatahan, and ~55 wt. % at Hekla, although petrographic and chemical evidence demonstrates oxide fractionation occurring earlier in both suites. Indeed, significant (titano)magnetite crystallisation and removal is necessary to impact $\delta^{51}V$ signatures whilst melt V concentration is relatively high. We speculate that magma chamber processes at Anatahan, where lavas are generally more evolved, are responsible for the lighter and more variable $\delta^{51}V$ in lavas with between 2 and 4 wt. % MgO compared to Hekla (Fig. 1b).

Self-consistent models of fractional crystallisation of cotectic phases have been constructed to account for systematic variations in major and trace element concentrations, as well as isotopic compositions in Hekla and Anatahan lavas (Fig. 2). Input parameters and results are provided in the Supplementary Information (Table S-3). Given the strong dependence of V partitioning on fO_2,

it is of particular interest to assess how the partition coefficient of V in (titano) magnetite differs between the two suites. A D^{mag}_V of 32 ± 4 is calculated from analyses of Anatahan lavas (de Moor *et al.*, 2005), a value that reproduces major, trace and isotopic trends very well. The required D^{mag}_V for Hekla lavas, however, must be significantly higher (~42) to reproduce the data. The relative difference in D^{mag}_V between the two suites is consistent with lower fO_2 at Hekla than Anatahan (*e.g.*, Toplis and Corgne, 2002). The same input parameters are used to perform Rayleigh calculations to estimate the bulk V isotope fractionation factor (Fig. 3). Both suites require large $\Delta^{51}V_{min\text{-}melt}$ fractionation factors on the order of $1000\ln\alpha_{min\text{-}melt}$ of -0.4 to -0.5 ‰. Arguably, a larger fractionation factor is required for Anatahan versus Hekla, however, the effect is subtle and difficult to resolve confidently within the current analytical precision.

Clearly, differences in mineral-melt bonding environment are key to producing large $\delta^{51}V$ fractionations. However, prior to significant (titano) magnetite crystallisation, $\delta^{51}V$ is identical within uncertainties in arc lavas, Icelandic lavas and MORB at similar MgO contents (Fig. 1). If interpreted as a direct fO_2 proxy, this conflicts with oxybarometry in peridotites, but is notionally consistent with their similar V/Sc ratios. This conclusion hinges, however, upon the assumption of a homogeneous source, both with respect to V/Sc and $\delta^{51}V$, an assumption that may be violated. For instance, $\delta^{51}V$ becomes isotopically lighter in progressively depleted (clinopyroxene-poor) peridotites (Prytulak *et al.*, 2013). This is an important observation because the arc mantle wedge has been inferred

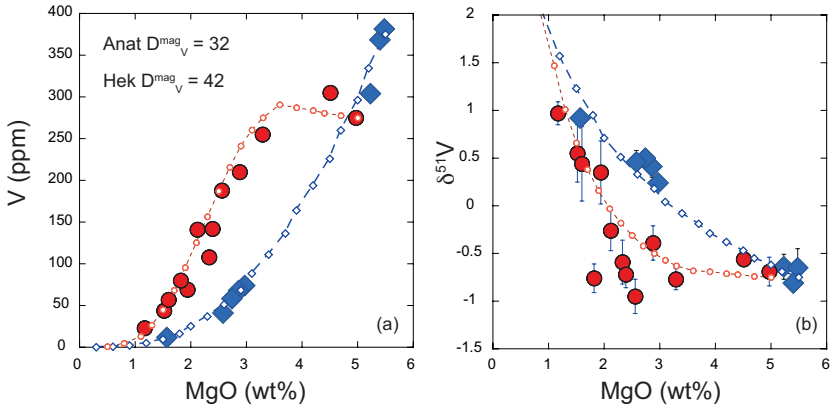

Figure 2 Cotectic fractional crystallisation models. Each small symbol represents a 5 % crystal fractionation increment. See Supplementary Information for input parameters. Symbols and uncertainties as in Figure 1.

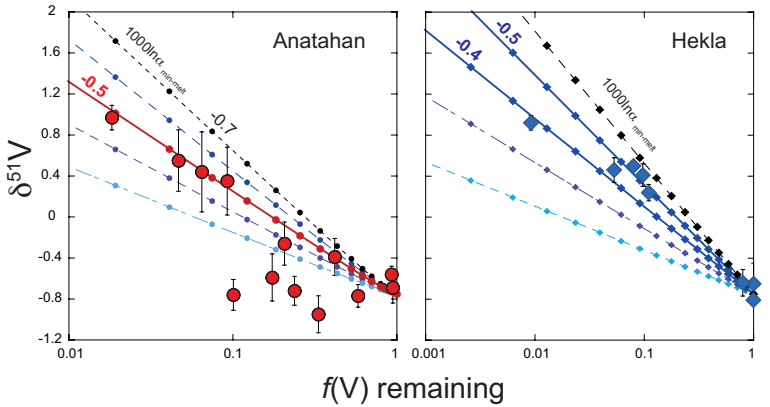

Figure 3 Rayleigh fractionation calculations with same parameters as Figure 2. Symbols and uncertainties as in Figure 1.

to be markedly depleted (*e.g.*, Woodhead, 1993; Nebel *et al.*, 2015) with respect to the source of MORB. In the absence of a common source, observations of similar V/Sc and $\delta^{51}V$ must be explained.

Primary arc magmas are notoriously rare, thus most information is garnered from basaltic andesites with Mg# too low (~0.5 assuming 20 % Fe^{3+}) to be in equilibrium with normal mantle (~0.9). Isotope fractionation during partial melting is possible, although high temperatures should minimise the effect. It is, however, perplexing that the well-constrained $\delta^{51}V_{MORB}$ is isotopically *lighter* than most peridotites and the bulk silicate Earth ($\delta^{51}V_{MORB}$ = -0.95 ± 0.13 ‰; $\delta^{51}V_{BSE}$ = -0.7 ± 0.2 ‰; Prytulak *et al.*, 2013). The peridotite trend towards lighter $\delta^{51}V$ with progressive depletion thus negates a simple explanation of isotope fractionation during melt extraction (Prytulak *et al.*, 2013). Given the strong effect of mineral-melt fractionation on $\delta^{51}V$, the potential for early phases to change the $\delta^{51}V$ of arc basalts should be considered. Water-rich magmas crystallise Cr-rich spinel before olivine (Feig *et al.*, 2010), potentially scavenging V. Oxide fractionation will drive remaining liquid to heavier $\delta^{51}V$, making early spinel crystallisation a viable mechanism to increase $\delta^{51}V$ in arc magmas. If arc magmas are derived from a depleted source with a lighter initial V isotope composition than the MORB source, it is therefore possible that the competing effects of source depletion and Cr-spinel fractionation result in similar $\delta^{51}V$ in mafic arc and non-arc magmas. Mineral separate data and the analysis of more primitive magmas are required to investigate this premise since it is currently not possible to evaluate the magnitude of isotopic increase due to early Cr-rich spinel, and/or partial melting, as there are no combined V concentration and $\delta^{51}V$ on spinel and scant peridotite whole rock data.

If arc magmas are derived from mantle more depleted than MORB, their sources should have lower $\delta^{51}V$ and V/Sc. The decrease of V/Sc in the source

will be exacerbated if prior melt-depletion occurs at high fO_2. Therefore, the observation of similar $\delta^{51}V$ and V/Sc ratios in high MgO lavas from both settings can be interpreted as evidence of melting of more depleted, oxidised sources in arcs. This concept is illustrated with two hypothetical sources in Figure 4a, with examples of simple forward trace element modal (Fig. 4b) and non-modal (Fig. 4c) melting models comparing V/Sc in lavas derived from these two sources. Overall, the effect of source depletion (*i.e.* less V) coupled with higher fO_2 (and thus lower D_V), can offset a more fertile (*i.e.* more V) less oxidised (higher D_V) source to yield similar V/Sc in resulting melts. Thus the confluence of $\delta^{51}V$ and V/Sc in arc and MORB lavas may paradoxically *require* differences in their source fO_2. Clearly, there are many possible solutions to such models, and the absolute values of V/Sc are very sensitive to input parameters (see Supplementary Information), however, given the assumption of a more oxidised, depleted arc source, the similarity of V/Sc in arc lavas and MORB at 10-15 % melt is relatively straightforward to reproduce.

Irrespective of the trade-offs involved in interpretation of relative oxidation states of arc and non-arc lavas, Rayleigh fractionation of oxide phases is dominantly responsible for the magnitude of observed V isotope fractionation in differentiating magmatic suites. Subtle fO_2-related variations are perhaps

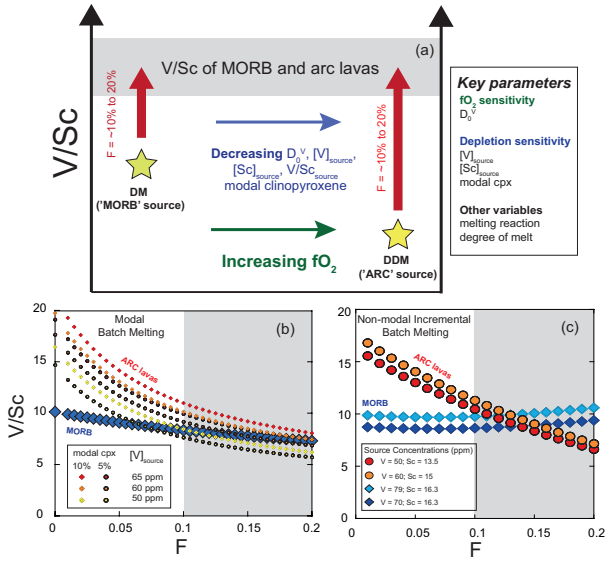

Figure 4 **(a)** Conceptual effect of depletion and oxidation on V/Sc ratios from two hypothetical spinel peridotite sources. **(b,c)** Modal and non-modal melting models for the sources in (a). Grey fields highlight reasonable melting degrees. Partition coefficients, modal compositions and melting reactions are detailed in the Supplementary Information. DM = depleted mantle, DDM = depleted MORB mantle, F = melt fraction.

overprinted onto first order bonding-environment induced fractionations, but these require a much richer understanding of $\delta^{51}V$ variations during magmatic processes to be applicable. Therefore, elemental partitioning of V yields a more direct relationship with fO_2 than the current understanding of V isotopes at high temperatures permits.

Acknowledgements

JP was funded by NERC postdoctoral fellowship NE/H01313X/2, with support of the Oxford laboratories from an Advanced ERC grant (NEWISOTOPEGEOSCIENCE) to ANH. PAS by an APA PhD scholarship and ANU Vice-Chancellor's Scholarship. We appreciate thoughtful reviews by F. Poitrasson and G. Mallmann. Tim Elliott is thanked for providing CIP samples. Although he may not necessarily agree with all the ideas presented, we thank Hugh O'Neill for many formative discussions.

Editor: Bruce Watson

Additional Information

Supplementary Information accompanies this letter at www.geochemicalperspectivesletters.org/article1708

Cite this letter as: Prytulak, J., Sossi, P.A., Halliday, A.N., Plank, T., Savage, P.S., Woodhead, J.D. (2017) Stable vanadium isotopes as a redox proxy in magmatic systems? *Geochem. Persp. Let.* 3, 75-84.

References

Brounce, M.N., Kelley, K.A., Cottrell, E. (2014) Variations in $Fe^{3+}/\sum Fe$ of Mariana arc basalts and mantle wedge fO_2. *Journal of Petrology* 55, 2513-2536.

Canil, D. (1997) Vanadium partitioning and the oxidation state of Archaean komatiite magmas. *Nature* 389, 842-845.

de Moor, J.M., Fischer, T.P., Hilton, D.R., Hauri, E., Jaffe, L.A., Camacho, J.T. (2005) Degassing at Anatahan volcano during the May 2003 eruption: implications from petrology, ash leachates, and SO_2 emissions. *Journal of Volcanology and Geothermal Research* 146, 117-138.

Elliott, T., Plank, T., Zindler, A., White, W.M., Bourdon, B. (1997) Element transport from slab to volcanic front at the Mariana arc. *Journal of Geophysical Research* 102, 14991-15019.

Feig, S.T., Koepke, J., Snow, J.E. (2010) Effect of oxygen fugacity and water on phase equilibria of a hydrous tholeiitic basalt. *Contributions to Mineralogy and Petrology* 160, 551-568.

Frost, D.J., McCammon, C.A. (2008) The redox state of Earth's mantle. *Annual Reviews in Earth and Planetary Science* 36, 389-420.

Kelley, K.A., Cottrell, E. (2009) Water and the oxidation state of subduction zone magmas. *Science* 325, 605-607.

Lee, C.-T.A., Brandon, A.D., Norman, M.D. (2003) Vanadium in peridotites as a proxy for paleo-fO2 during partial melting: prospects, limitations, and implications. *Geochimica et Cosmochimica Acta* 67, 3045-3064.

Lee, C.-T.A., Leeman, W.P., Canil, D., Li, Z.-X.A. (2005) Similar V/Sc systematics in MORB and arc basalts: implications for the oxygen fugacities of their mantle source regions. *Journal of Petrology* 46, 2313-2336.

Lee, C.-T.A., Luffi, P., Le Roux, V., Dasgupta, R., Albarede, F., Leeman, W.P. (2010) The redox state of arc mantle using Zn/Fe systematics. *Nature* 468, 681-685.

Mallmann, G., O'Neill, H.St.C. (2009) The crystal/melt partitioning of V during mantle melting as a function of oxygen fugacity compared with some other elements (Al, P, Ca, Sc, Ti, Cr, Fe, Ga, Y, Zr, Nb). *Journal of Petrology* 50, 1765-1794.

Moune, S., Sigmarsson, O., Thordarson, T., Gauthier, P.-J. (2007) Recent volatile evolution in the magmatic system of Hekla volcano, Iceland. *Earth and Planetary Science Letters* 255, 373-389.

Nebel, O., Sossi, P.A., Benard, A., Wille, M., Vroon, P.Z., Arculus, R.J. (2015) Redox-variability and controls in subduction zones from an iron-isotope perspective. *Earth and Planetary Science Letters* 423, 142-151.

Nielsen, S.G., Prytulak, J., Halliday, A.N. (2011) Determination of precise and accurate $^{51}V/^{50}V$ isotope ratios by MC-ICP-MS, part 1: chemical separation of vanadium and mass spectrometric protocols. *Geostandards and Geoanalytical Research* 35, 293-306.

O'Neill, H.St.C., Navrotsky, A. (1984) Cation distributions and thermodynamic properties of binary spinel solid solutions. *American Mineralogist* 69, 733-753.

Pauling, L. (1929) The principles determining the structure of complex ionic crystals. *Journal of American Chemical Society* 51, 1010-1026.

Prytulak, J., Nielsen, S.G., Halliday, A.N. (2011) Determination of precise and accurate $^{51}V/^{50}V$ isotope ratios by multi-collector ICP-MS, part 2: isotopic composition of six reference materials plus the Allende chondrite and verification tests. *Geostandards and Geoanalytical Research* 35, 307-318.

Prytulak, J., Nielsen, S.G., Ionov, D.A., Halliday, A.N., Harvey, J., Kelley, K.A., Niu, Y.L., Peate, D.W., Shimizu, K., Sims, K.W.W. (2013) The stable vanadium isotope composition of the mantle and mafic lavas. *Earth and Planetary Science Letters* 365, 177-189.

Righter, K., Sutton, S.R., Newville, M., Le, L., Schwandt, C.S., Uchida, H., Lavina, B., Downs, R.T. (2006) An experimental study of the oxidation state of vanadium in spinel and basaltic melt with implications for the origin of planetary basalt. *American Mineralogist* 91, 1643-1656.

Savage, P.S., Georg, R.B., Williams, H.M., Burton, K.W., Halliday, A.N. (2011) Silicon isotope fractionation during magmatic differentiation. *Geochimica et Cosmochimica Acta* 75, 6124-6139.

Schuessler, J.A., Schoenberg, R., Sigmarsson, O. (2009) Iron and lithium isotope systematics of the Hekla volcano, Iceland – evidence for Fe isotope fractionation during magma differentiation. *Chemical Geology* 258, 78-91.

Shervais, J.W. (1982) Ti-V plots and the petrogenesis of modern and ophiolitic lavas. *Earth and Planetary Science Letters* 59, 101-118.

Shorttle, O., Moussallam, Y., Hartley, M.E., Maclennan, J., Edmonds, M., Murton, B.J. (2015) Fe-XANES analyses of Reykjanes Ridge basalts: Implications for oceanic crust's role in the solid Earth oxygen cycle. *Earth and Planetary Science Letters* 427, 272-285.

Sossi, P.A., Foden, J.D., Halverson, G.P. (2012) Redox-controlled iron isotope fractionation during magmatic differentiation: an example from the Red Hill intrudion, S. Tasmania. *Contributions to Mineralogy and Petrology* 164, 757-772.

Toplis, M.J., Corgne, A. (2002) An experimental study of element partitioning between magnetite, clinopyroxene and iron-bearing silicate liquids with particular emphasis on vanadium. *Contributions to Mineralogy and Petrology* 144, 22-37.

Wade, J.A., Plank, T., Stern, R.J., Tollstruo, D.L., Gill, J.B., O'Leary, J.C., Eiler, J.M., Moore, R.B., Woodhead, J.D., Trusdell, F., Fischer, T.P., Hilton, D.R. (2005) The May 2003 eruption of Anatahan volcano, Mariana Islands: geochemical evolution of a silicic island-arc volcano. *Journal of Volcanology and Geothermal Research* 146, 139-170.

Waters, L.E., Lange, R.A. (2016) No effect of H_2O degassing on the oxidation state of magmatic liquids. *Earth and Planetary Science Letters* 447, 48-59.

Woodhead, J., Eggins, S., Gamble, J. (1993) High field strength and transition element systematics in island arc and back-arc basin basalts: evidence for multi-phase melt extraction and a depleted mantle wedge. *Earth and Planetary Science Letters* 114, 491-504.

Stable vanadium isotopes as a redox proxy in magmatic systems?

J. Prytulak[1*], P.A. Sossi[2], A.N. Halliday[3], T. Plank[4], P.S. Savage[5], J.D. Woodhead[6]

Supplementary Information

The Supplementary Information includes:

- Methods and Model Descriptions
- Tables S-1 to S-4
- Supplementary Information References

Methods and Model Descriptions

Table S-1 presents a compilation of published major and trace element and radiogenic isotope data on the samples used in this study. We have also compiled available information on other stable isotope systems such as Mo (Freymuth *et al.*, 2015; Yang *et al.*, 2015), Zn (Chen *et al.*, 2013), Cu (Savage *et al.*, 2015), and Tl (Prytulak *et al.*, 2013).

Measurement of vanadium isotopes

Table S-2 presents new whole rock stable vanadium isotope data. Measurement took place at University of Oxford and Imperial College London following the protocols outlined in Nielsen *et al.* (2011).

Briefly, 50-150 mg of sample were dissolved with standard HF-HNO_3 techniques and put through a seven-column procedure to separate V quantitatively from Cr, Ti and other matrix elements. Isotope ratio measurement was conducted

1. Department of Earth Science and Engineering, Imperial College London, UK
* Corresponding author (email: j.prytulak@imperial.ac.uk)
2. Institut de Physique du Globe de Paris, France
3. Department of Earth Science, University of Oxford, UK
4. Lamont-Doherty Earth Observatory, Columbia University, USA
5. Department of Earth and Environmental Sciences, University of St. Andrews, UK
6. School of Earth Sciences, University of Melbourne, Australia

on Nu Plasma HR machines at both Oxford and Imperial, using a 10^9 Ω resistor to collect ^{51}V and standard 10^{11} Ω resistors for all other masses. Sample solutions were 5 ppm and total procedural blanks were <1.5 ng, which is negligible compared to the amount of V processed (5-20 µg).

Sample measurements were contemporaneous with those of USGS reference materials and verification tests presented in Prytulak *et al.* (2011). Many of the samples were measured multiple times and across both Oxford and Imperial as the first inter-laboratory vanadium isotope effort (Table S-2). Measurements of the secondary V solution standard, BDH, were $\delta^{51}V$ = -1.17 ± 0.17 2sd (n = 1329) over the Oxford-Imperial cross calibration period. The isotopic offset of AA-BDH has been confirmed in subsequent studies using vastly different measurement protocols and consuming significantly less vanadium (Nielsen *et al.*, 2016; Wu *et al.*, 2016).

Modelling $\delta^{51}V$-MgO-V during magmatic differentiation

Both lava suites are modelled assuming that they are related by fractional crystallisation using the equations of Shaw (1970). Such a relationship has been demonstrated for Anatahan lavas by Wade *et al.* (2005). This assumption does not hold in detail for Hekla, where there is evidence for mixing between basaltic andesites and dacites (*e.g.*, Sigmarsson *et al.*, 1992), but is an adequate approximation. Note that (titano)magnetite is always crystallising in the investigated lavas at Hekla due to their Fe-rich nature (*e.g.*, Sigmarsson *et al.*, 1992). The delayed onset of major magnetite fractionation in Anatahan lavas may be due to suppression by water (*e.g.*, Feig *et al.*, 2010), although this remains controversial.

The objective of the calculations is not to model all aspects of magmatic differentiation, but rather to produce an internally consistent model whereby the chemical trends of Mg, Fe, V (and its isotopes) and inferred melt fractions are reproduced. As a first step, the degree of melt remaining (the operative variable in the modal calculations) is calibrated against natural samples by their MgO-Rb systematics. For fractional crystallisation, the concentration of a perfectly incompatible element (*i.e.* $D_{Min\text{-}Melt} = 0$) in the melt is given by $C_l = C_0/F$, where C_0 is the bulk concentration and F the melt fraction. The melt fraction calculated from Rb abundances (F_{Rb}) shows a linear relationship with MgO for both suites, where $F_{Rb} = 0.19 \times$ MgO wt. %. This is used to anchor the model in terms of Mg-Fe evolution, where both elements are treated as trace elements for simplicity. Modelling of the two evolving suites was performed at 5 % intervals of melt remaining (F). At Anatahan, mineral assemblages from de Moor *et al.* (2005) of 60 % plagioclase, 15 % opx and cpx with 5-10 % Fe-Ti oxides is used as a guide. The onset of significant (titano)magnetite crystallisation is estimated at 4 wt. % MgO from the precipitous decrease in V concentration. The fractionating assemblage at Hekla consists of olivine (and later orthopyroxene), plagioclase, clinopyroxene and titanomagnetite (Sigmarsson *et al.*, 1992), though the proportions are not reported, they are adjusted so as to fit the MgO-FeO evolution defined by the whole rocks.

The V partition coefficient for magnetite at Anatahan is calculated from the measurements of de Moor *et al.* (2005), $D^{Mag}_V = 32$. The D_V for magnetite at Hekla is determined by the best fit to the data ($D^{Mag}_V = 42$). For pyroxenes, values for the NNO experiments of Mallmann and O'Neill (2009) were used.

We use the most primitive (highest V contents) lavas from each suite as a starting point. Clearly Hekla (375 ppm V) has less evolved magmas than Anatahan (275 ppm V), but since their most primitive lavas available have similar $\delta^{51}V$, we use $\delta^{51}V$ = -0.75 as a starting composition for both. We prescribe initial V, MgO and FeO contents according to the most magnesian lava in the suite.

Temperatures are important when evaluating bulk isotope fractionation factors, particularly since contrasting temperatures are expected between the two suites of lavas. de Moor *et al.* (2005) used 2-pyroxene equilibrium thermometry to estimate magmatic temperatures of 1050-1100 °C. This matches well with the empirical relationship developed for mafic magmas (T (1atm) = 1000 + 20*MgO) from Nisbet (1982). This relationship is used to estimate similar magmatic temperatures at Hekla. Table S-3 tabulates the results of the fractional crystallisation model and gives all input parameters.

The extent of vanadium isotope fractionation is calculated by the Rayleigh distillation equation, $\delta^{51}V_{Melt} = \delta^{51}V_{Bulk} + \Delta^{51}V_{Min\text{-}Melt}\ln(F_V)$, where F_V is the fraction of V remaining in the liquid. As each phase partitions V differently, a weighting factor, W, is given by $W_n = (P_nD_n)/\sum_n(P,D)$, where P is the modal proportion of phase, n, and D is the partition coefficient. When (titano)magnetite crystallises, it hosts >75 % of the V budget, thereby controlling its isotope fractionation in magmatic suites.

Modelling V/Sc ratios with variable fO_2 and source depletion

1. Model Rationale. Here we detail the example forward models shown in Figure 4b,c. The majority of melt in both subduction zone and MORB are generated at pressures in the spinel stability field, thus we focus on the melting of spinel peridotite. Furthermore, the REE pattern of both suites of lavas are flat and lack obvious evidence for involvement of garnet in their sources.

The models explore aspects of the parameter space to give a sense of the dominant sensitivities and are intended to be illustrative rather than quantitatively comparable to natural samples. We focus on comparing the expected V/Sc ratios of lavas from a 'MORB' source and an 'ARC' source. The most critical assumption is that the arc source is one log unit more oxidised than the MORB source. Internally consistent partition coefficients for V and Sc from Mallmann and O'Neill (2009) are used, which have data for the same starting composition with variable fO_2 and a focus on vanadium partitioning. We use their experiments for FMQ + 0.3 (experiments V1, V7, V8) and FMQ +1.3 (experiments V1, V7, V5). Because the degrees of melting in arc and MORB (and Iceland) are large (>10 %), batch and fractional melting models should yield similar results for liquid compositions. Given that neither V nor Sc are highly incompatible, the residues from a batch and fractional approach will not be markedly different

either. Simple modal batch melting is used to explore the effects of changing modal compositions and source concentrations (Fig. 4b) and results are compared with a more detailed incremental non-modal melting approach that specifically models residual concentrations and recalculated partition coefficients and modal abundances at every step (Fig. 4c).

2. Modal batch melting. The depleted mantle MORB source is modelled with the following parameters from Salters and Stracke (2004): source [V] = 79 ppm, [Sc] = 16.3 ppm. Modal composition is 60 % olivine, 20 % orthopyroxene, 15 % clinopyroxene and 5 % spinel. Even with a set choice for partition coefficients, the bulk D_V in a spinel lherozolite assemblage varies a great deal depending on modal abundances. Two scenarios of 5 % and 10 % modal clinopyroxene in the source of arc lavas are explored. Curves calculated for how V/Sc ratio changes with degree of melting in MORB and arc lavas are depicted in Figure 4b.

3. Non-modal incremental melting. A more realistic scenario with the non-modal melting equations of Shaw (1970) are explored in Figure 4c. Self-consistent V and Sc partition coefficients (Table S-4) from Mallmann and O'Neill (2009) and the melting reaction coefficients of Kinzler (1997) experiment L134 to L138 (0.13opx + 0.89cpx + 0.12sp = liquid + 0.13ol) are used. This experiment was chosen because it is relevant for spinel peridotite melting up to 24 % at 1.5 GPa, conditions reasonable for the exploratory calculations here. Each 1 % increment of melt is formed and removed, and subsequent modal abundances, residual concentration of V and Sc, and bulk D_V and D_{Sc} are recalculated at each step. Table S-4 gives an example of how modes and bulk partition coefficients change with progressive melting.

Absolute values of V/Sc change dependent on the input parameters such as source concentrations and partition coefficients, when comparing lavas of similar, reasonable melting degrees (*i.e.* 10-20 %). Critically, a common feature of all forward models, assuming that arc lavas generally derive from a more depleted, oxidised source compared to MORB, is the overlap in V/Sc ratio due to decreasing V bulk partition coefficient and source V concentration in arc sources. This can counterbalance the higher V source concentration and V bulk partition coefficient of more fertile sources, leading to the generation of similar V/Sc in both settings. The variation in V/Sc with degree of melt in MORB is muted compared to arc lavas due to the more compatible behaviour of V in our models which means, although $D_V < D_{Sc}$, the two absolute values are similar. It is interesting to note that the V/Sc ratio of arc lavas from this calculation are in good agreement with $V/Sc_{MORB} = 6.74 \pm 1.11$ determined by Li and Lee (2004) from a global database. The V/Sc ratios of lavas from our 'MORB' source do not reproduce this value very well, but can be shifted to higher and lower values simply by choice of starting composition (Fig. 4c). Models incorporating a greater pressure range extending into the garnet stability field may also be able to better reconcile this difference, however, this is beyond the scope of the current contribution.

Letter Geochemical Perspectives Letters

Tables S-1 to S-4

Table S-1 Background chemical data.

A. MAJOR ELEMENTS													
	eruption age	SiO_2	TiO_2	Al_2O_3	Fe_2O_3	MnO		MnO	CaO	Na_2O	K_2O	P_2O_5	LOI
Hekla													
hek 6	1913 AD	46.20	4.508	13.73	17.28	0.254		5.40	9.45	2.74	0.64	0.538	-0.40
hek 12	1913AD	46.42	4.469	13.59	17.18	0.259		5.23	9.22	2.81	0.67	0.566	-0.29
hek 5	1913AD	46.47	4.493	13.85	17.28	0.253		5.48	9.53	2.76	0.63	0.529	-0.38
hek 14	1991 AD	53.71	2.120	14.80	13.26	0.274		2.97	6.98	3.95	1.23	1.066	-0.15
hek 17	1980 AD	54.57	2.060	14.75	13.05	0.276		2.86	6.80	3.94	1.26	1.007	-0.13
hek 16	1980 AD	54.81	1.961	14.90	12.71	0.275		2.74	6.67	4.02	1.28	0.929	-0.11
hek 21	1390 AD	55.64	1.773	15.14	12.56	0.273		2.58	6.34	4.12	1.35	0.865	-0.09
hek 15	1980 AD	59.64	1.164	15.22	10.27	0.248		1.57	5.07	4.55	1.66	0.425	0.03
Anatahan													
AN-10		63.91	0.75	15.47	7.026	0.20		1.52	4.56	4.38	1.88	0.30	
Anat9		65.06	0.83	15.00	7.515	0.19		1.17	4.22	4.27	2.05	0.30	
04-Anat-01		59.51	0.87	17.14	8.163	0.21		1.94	5.56	4.02	1.49	0.31	
04-Anat-03		56.35	0.75	18.89	7.899	0.17		2.12	8.17	3.60	1.26	0.22	
04-Anat-04		54.03	0.78	19.41	8.688	0.18		2.56	9.08	3.44	1.00	0.19	
AN-2		52.31	0.71	21.18	8.772	0.16		2.88	10.59	2.76	0.51	0.12	
AN-1		51.66	0.73	18.54	10.340	0.19		4.97	10.34	2.53	0.57	0.13	
AN-8		49.28	0.68	20.09	10.649	0.19		4.51	11.81	2.22	0.46	0.11	
Anat4-s		61.26	0.80	15.67	8.360	0.21		1.82	5.44	3.99	1.52	0.32	
AN-12D		62.82	0.83	15.12	8.270	0.21		1.60	4.82	4.33	1.67	0.32	
AN-7		53.49	0.79	18.63	10.370	0.20		3.29	9.33	3.06	0.68	0.16	
Anat-26-01		60.29	0.84	16.10	8.568	0.20		2.33	6.04	3.73	1.37	0.32	
Anat-26-02		58.36	0.88	16.13	9.040	0.22		2.39	6.22	4.41	1.36	0.25	
Mariana Central Island Province													
ALAM 2		54.95	0.783	17.4	9.58	0.184		4.4	8.98	2.98	0.944	0.145	
AGR 8B		50.5	0.726	20.2	9.83	0.186		3.55	11.15	2.58	0.889	0.175	
PAG 1		51.34	0.908	15.87	12.19	0.218		5.45	10.6	2.8	0.749	0.142	
PAG 3		51.64	0.925	15.73	12.23	0.218		5.25	10.25	2.72	0.78	0.149	
GUG 4		52.37	0.824	17.54	10.26	0.197		5.22	10.41	2.64	0.549	0.105	

Letter Geochemical Perspectives Letters

A. MAJOR ELEMENTS

	eruption age	SiO_2	TiO_2	Al_2O_3	Fe_2O_3	MnO	MnO	CaO	Na_2O	K_2O	P_2O_5	LOI
GUG 9		50.985	0.82	19.6	10.07	0.18	4.23	11.05	2.56	0.433	0.087	
MM-92-6		55.24	0.872	16.49	10.67	0.236	3.15	7.68	3.56	1.41	0.269	
GUG3		51.61	0.858	19.75	9.93	0.191	3.36	10.5	2.69	0.908	0.174	
GUG11		52.96	0.807	19.88	9.32	0.177	3.38	10.22	2.95	0.507	0.098	
ALAM5		53.39	0.815	17.17	10.05	0.19	4.86	9.97	2.7	0.835	0.144	
URA6		59.92	0.826	15.39	9.99	0.234	2.25	6.2	3.85	1.099	0.186	
SAG1		53.37	0.777	16.23	9.83	0.186	5.57	10.45	2.71	0.716	0.126	
GUG13		51.78	0.807	19.94	9.67	0.179	3.47	10.66	2.55	0.442	0.087	
GUG12		52.16	0.814	20.04	9.73	0.183	3.49	10.73	2.67	0.448	0.089	
URA5		53.57	0.628	16.63	9.61	0.184	6.13	10.52	2.29	0.53	0.094	
URA7		54.17	0.775	19.2	9.73	0.193	2.712	9.64	2.88	0.756	0.134	
URA12		53.77	0.75	19.62	9.55	0.188	2.68	9.93	2.81	0.705	0.128	
AGR1		51.58	0.752	20.19	9.77	0.188	3.04	10.71	2.72	1.03	0.189	
AGR2		50.94	0.794	16.84	12.45	0.235	4.98	10.46	2.85	0.744	0.147	

B. TRACE ELEMENTS

	Zn (Savage)	Zn (ICP)	Li	Be	Sc	V	Cr	Co	Ni	Cu	Cu	Rb	Sr	Y	Zr	Nb	Cs	Tl	Ba	La	Ce	Pr	Nd	Sm	Eu	Tb	Ga	Gd	Dy	Ho	Er	Yb	Lu	Hf	Ta	Pb	Th	U
	XRF	ppm	ppm	ppm	ppm	ppm	ppm	ppm	ppm	ppm	(savage XRF)	ppm	ppm	ppm	ppm	ppm	ppm	ppb	ppm	ppm	ppm	ppm	ppm	ppm	ppm	ppm	ppm	ppm	ppm	ppm	ppm	ppm	ppm	ppm	ppm	ppm	ppm	ppm
Hekla																																						
hek 6	134.00	136.56	8.04	1.96	34.53	368.43	12.09	47.43	13.64	42.01	38.00	11.83	363.83	46.23	271.21	43.78	0.15	20.29	178.08	27.14	63.19	8.72	38.77	9.57	3.14	1.62	23.93	10.03	9.11	1.79	4.67	4.06	0.59	6.82	2.99	1.72	2.20	0.67
hek 12							2.00	31.00			26.00	14.00	371.00	49.20	275.00	41.00																							
hek 5	136.00	139.95	8.18	1.89	34.80	381.44	15.24	48.81	17.14	50.80	47.00	12.04	370.35	46.50	272.22	43.66	0.15	21.96	177.77	27.07	62.86	8.69	38.25	9.50	3.10	1.60	24.42	9.90	8.97	1.76	4.60	3.99	0.58	6.69	2.95	1.70	2.14	0.66
hek 14	163.00	188.23	15.63	3.32	22.40	74.02	16.90	18.08	4.24	15.56	17.00	25.20	400.40	77.67	476.38	66.16	0.32	48.68	332.54	51.76	117.54	15.93	67.18	16.04	4.81	2.59	27.59	16.25	14.43	2.83	7.41	6.49	0.96	11.14	4.14	3.39	4.54	1.37
hek 17	135.00	186.71	15.81	3.32	22.45	67.80	5.26	16.71	4.02	15.25	15.00	25.67	388.72	76.94	484.92	66.83	0.32	50.64	335.54	51.76	116.91	15.78	65.90	15.75	4.69	2.54	27.40	15.92	14.22	2.79	7.33	6.44	0.95	11.23	4.15	3.40	4.57	1.39
hek 16	163.00	189.30	16.22	3.47	22.23	58.24	9.29	15.69	3.62	14.32	16.00	26.33	393.96	77.60	494.48	67.87	0.33	50.59	344.19	52.40	118.18	15.90	66.34	15.86	4.75	2.56	27.68	15.97	14.35	2.82	7.48	6.61	0.97	11.55	4.22	3.49	4.70	1.42
hek 21	162.00	188.91	15.98	3.60	20.75	41.11	5.42	14.77	3.18	14.85	18.00	27.31	393.07	77.98	509.15	68.05	0.35	53.79	353.76	53.27	119.98	16.02	66.43	15.82	4.70	2.55	27.75	15.86	14.34	2.83	7.46	6.66	0.98	11.81	4.20	3.67	4.88	1.46
hek 15	163.00	195.84	20.58	4.28	19.44	11.71	2.79	8.47	4.01	10.17	13.00	34.39	368.61	82.67	627.62	78.59	0.44	59.17	433.10	59.43	131.16	17.12	68.91	16.01	4.74	2.63	30.27	15.96	15.00	3.00	8.13	7.55	1.12	14.64	4.84	4.24	6.10	1.83
Anatahan																																						
AN-10			13.71	1.07	20.48	44	0.20	9.15	1.46	14.74		36.77	323.09	43.12	140.94	3.37	0.81	114	478.768	15.07	32.58	4.79	21.27	5.64	1.60	1.13		6.62	6.87	1.49	4.21	4.26	0.67	3.72	0.27	5.55	2.22	0.92
Anat9			13.75	1.27	20.53	23	5.30	11.65	2.33	24.67		42.58	302.48	46.95	170.80	3.64	0.94	106	538.275	15.95	33.66	4.92	22.58	6.08	1.76	1.24		7.32	7.78	1.65	4.76	4.77	0.76	4.51	0.27	7.13	2.67	1.11
04-Anat-01			11.64	0.99	23.10	69	0.52	13.72	0.56	32.86		28.68	342.00	39.07	117.70	2.94	0.72	97	405.365	12.61	27.74	4.27	18.80	5.10	1.58	1.01		6.02	6.33	1.37	3.87	3.86	0.61	3.32	0.20	4.95	1.84	0.73

Geochem. Persp. Let. (2017) 3, 75-84 | doi: 10.7185/geochemlet.1708 SI-8

B. TRACE ELEMENTS

	Zn (Savage)	Zn (ICP)	Li	Be	Sc	V	Cr	Co	Ni	Cu	Cu	Rb	Sr	Y	Zr	Nb	Cs	Tl	Ba	La	Ce	Pr	Nd	Sm	Eu	Tb	Ga	Gd	Dy	Ho	Er	Yb	Lu	Hf	Ta	Pb	Th	U
	XRF	ppm	ppm	ppm	ppm	ppm	ppm	ppm	ppm	ppm	(savage XRF)	ppm	ppm	ppm	ppm	ppm	ppm	ppb	ppm	ppm	ppm	ppm	ppm	ppm	ppm	ppm	ppm	ppm	ppm	ppm	ppm	ppm	ppm	ppm	ppm	ppm	ppm	ppm
04-Anat-03			8.56	0.77	22.07	141	0.45	17.19	1.45	62.83		23.52	417.00	29.69	90.93	2.23	0.60	75	331.203	9.82	21.36	3.13	14.45	3.90	1.27	0.77		4.57	4.85	1.04	2.95	2.93	0.46	2.57	0.15	4.09	1.44	0.59
04-Anat-04			7.77	0.66	25.67	188	1.39	21.23	2.74	63.30		20.32	428.00	27.34	79.49	2.59	0.53	66	279.978	8.19	17.88	2.72	12.35	3.41	1.15	0.69		4.05	4.38	0.95	2.70	2.69	0.42	2.24	0.18	3.50	1.23	0.51
AN-2			5.28	0.45	25.47	210	4.32	30.64	9.90	85.40		9.50	445.44	20.60	50.06	1.14	0.24	38	191.482	5.25	11.52	1.83	8.60	2.49	0.90	0.54		3.10	3.38	0.72	2.03	2.07	0.32	1.41		2.34	0.66	0.26
AN-1			5.25	0.47	31.74	275	17.93	31.56	17.84	116.05		11.58	381.51	20.65	51.78	1.23	0.28	26	198.584	5.69	12.30	1.88	8.78	2.52	0.87	0.54		3.11	3.42	0.74	2.08	2.10	0.33	1.49	0.09	2.42	0.86	0.31
AN-8			4.40	0.37	32.30	305	4.42	33.04	14.72	103.63		10.55	447.37	16.13	35.35	0.84	0.21	24	147.884	4.89	10.38	1.65	7.30	2.07	0.77	0.43		2.51	2.64	0.57	1.60	1.57	0.25	1.02	0.06	2.37	0.62	0.23
Anat4-s			12.04	1.06	23.44	80	0.77	15.77	5.25	38.81		30.54	339.63	41.56	126.31	2.88	0.76		434.741	13.70	29.13	4.28	19.90	5.46	1.68	1.11		6.57	6.97	1.49	4.26	4.16	0.68	3.41	0.22	5.75	2.02	0.79
AN-12D			8.18	1.04	23.14	57	0.07	12.22	0.38	31.58		30.59	331.28	44.18	132.55	3.17	0.63		444.328	13.99	30.25	4.57	20.74	5.61	1.69	1.16		6.86	7.02	1.51	4.35	4.32	0.69	3.71	0.23	5.56	2.08	0.84
AN-7			6.36	0.51	30.27	255	2.32	25.68	6.08	105.06		11.73	414.14	24.72	61.72	1.20	0.18		240.807	5.79	13.39	2.04	9.67	2.89	0.99	0.63		3.61	3.97	0.86	2.42	2.43	0.39	1.67	0.11	2.34	0.80	0.35
Anat-26-01			12.44	0.89	24.69	108	2.72	14.92	0.86	39.79		28.31	345.00	35.04	105.54	2.54	0.68		374.247	11.34	24.78	3.65	16.79	4.56	1.43	0.91		5.37	5.66	1.23	3.46	3.48	0.55	2.99	0.18	4.81	1.69	0.68
Anat-26-02			8.10	0.82	26.30	142	0.96	22.37	2.98	66.39		23.62	366.00	33.28	97.55	2.48	0.58		356.779	10.77	24.05	3.70	16.82	4.59	1.44	0.89		5.24	5.50	1.18	3.38	3.44	0.54	2.80	0.17	4.32	1.53	0.63
Mariana Central Island Province																																						
ALAM 2		78.7			32	218	19.7		20			16.34	303	26.7	82.9	1.305	0.605	59	251	5.90	14.04	2.17	10.33	3.05	0.967	0.727	17.24	3.86	4.29	0.933	2.69	2.73	0.443	2.33	0.093	3.14	0.816	0.409
AGR 8B		76.1			30.45	257	6.5		12.3			19.89	395	18.1	59.2	1.126	0.463	54	165	7.45	15.76	2.34	10.73	2.79	0.992	0.563	18.71	3.17	3.16	0.667	1.87	1.86	0.288	1.60	0.088	1.79	0.894	0.377
PAG 1		98.7			41.0	386.1	33.706		22.6			11.92	334			1.016	0.524	25	221	5.242	12.051	1.913	9.225	2.827	0.960	0.584	17.45	3.380	3.749	0.789	2.218	2.219	0.334	1.579	0.073	2.801	0.542	0.263
PAG 3		100.0			41.3	373	44.9		26.4			12.46	317	23.2	60.8	0.965	0.608	27	230	5.18	12.45	1.95	9.57	2.95	1.015	0.670	17.15	3.69	3.93	0.853	2.40	2.36	0.369	1.80	0.071	2.71	0.537	0.280
GUG 4		86.4			34.8	258.9	37.4		24			8.07	291	22.8	57.9	0.808	0.357	44	167	3.55	9.11	1.50	7.58	2.39	0.861	0.600	17.5	3.23	3.57	0.791	2.26	2.30	0.365	1.63	0.071	2.42	0.350	0.201
GUG 9		81.0			30.1	272.4	12.3		14.9			6.53	299	20.1	50.4	0.731	0.297	36	139	2.85	7.63	1.30	6.57	2.14	0.809	0.547	18.5	2.86	3.29	0.727	2.11	2.07	0.331	1.42	0.061	2.03	0.271	0.147
MM-92-6		116.1			31.8	204.5			11.1			31.45	324	29.8	96.3	1.856	0.733	115	277.7	11.41	23.98	3.53	15.88	4.11	1.373	0.874	18.22	4.84	4.93	1.058	2.98	2.94	0.472	2.59	0.117	3.01	1.422	0.563
GUG3		82.4			28.6	278.6	4.7		12.6			16.9	401	23.0	66.3	1.241	0.467	67	217	7.40	15.86	2.40	11.11	3.08	1.084	0.657	17.7	3.65	3.81	0.816	2.30	2.29	0.356	1.78	0.092	2.82	0.760	0.352
GUG11		77.8			28.3	241	4.3		15.2			7.2	306	23.5	60.0	0.699	0.271	31	190	3.18	8.53	1.46	7.47	2.43	0.920	0.626	18.44	3.19	3.72	0.830	2.38	2.46	0.391	1.70	0.069	2.44	0.297	0.175
ALAM5		82.0			36.5	264	22.1		18.4			15.41	307	24.1	74.4	1.244	0.589	56	238	5.85	13.51	2.12	10.12	2.99	1.011	0.693	15.55	3.73	4.10	0.890	2.54	2.53	0.394	2.18	0.095	3.24	0.824	0.395
URA6		111.4			31.1	120	0.01		5.4			18.32	319	36.4	96.1	2.107	0.675	80	424	10.05	22.20	3.19	14.92	4.30	1.448	1.014	17.29	5.33	6.04	1.345	3.85	3.92	0.617	2.78	0.143	4.23	1.501	0.511
SAG1		77.8			34.8	233	63.1		29.4			9.45	352	23.5	68.5	1.641	0.353	44	253	6.17	13.98	2.14	10.01	2.86	1.014	0.644	16.27	3.51	3.75	0.787	2.29	2.28	0.350	1.90	0.120	3.63	0.886	0.366
GUG13		77.5			29.5	265	1.7		12			6.06	303	21.6	53.4	0.674	0.223	15	162	2.75	7.53	1.28	6.59	2.21	0.829	0.573	18.44	2.96	3.51	0.781	2.17	2.22	0.358	1.55	0.059	1.92	0.244	0.146
GUG12		78.6				285.7	53.2		28.9			7.35	281	21.7	53.5	0.720	0.198	49	172	3.26	8.43	1.40	7.08	2.27	0.841	0.559	16.9	2.94	3.38	0.743	2.15	2.18	0.345	1.50	0.066	1.81	0.316	0.206
URA5		72.3			39.65	235	48.9		26.5			8.15	307	20.2	49.0	1.044	0.365	38	198	4.45	10.17	1.54	7.25	2.15	0.814	0.528	14.17	2.80	3.19	0.696	1.99	2.05	0.324	1.37	0.072	2.06	0.657	0.240
URA7		85.8			29.9	232	2.4		11			12.01	384	24.0	62.6	1.663	0.401	47	290	7.97	16.80	2.41	10.75	2.97	1.066	0.699	18.2	3.68	4.19	0.882	2.56	2.55	0.406	1.76	0.101	2.76	1.214	0.399
URA12		82.6			30.1	208	2.3		9.3			11.9	398	23.0	59.4	1.596	0.390	51	245	7.29	15.57	2.21	9.98	2.79	1.004	0.638	18.09	3.41	3.80	0.827	2.34	2.35	0.385	1.66	0.092	2.59	1.157	0.373
AGR1		75.7				246	5.2		9.7			22.5	394				0.526		181								20.16					0.68						
AGR2		89.6				341	5.7		12.4			12.96	344	20.1	51.9	1.007	0.160	23	158	6.84	14.71	2.24	10.48	2.90	1.028	0.603	17.11	3.33	3.47	0.741	2.09	2.01	0.316	1.52	0.065	1.83	0.822	0.313

C. ISOTOPIC DATA

	$^{87}Sr/^{86}Sr$	$^{143}Nd/^{144}Nd$	$^{206}Pb/^{204}Pb$	2sd	$^{207}Pb/^{204}Pb$	2sd	$^{208}Pb/^{204}Pb$	2sd	$d^{30}Si$	2sd	$d^{29}Si$	2sd	Mo	$d^{98}Mo$	2se	$d^{66}Zn$	$d^{67}Zn$	$d^{68}Zn$	$d^{65}Cu$	2sd	$e^{205}Tl$	2sd
Hekla													ug/g									
hek 6									-0.31	0.09	-0.16	0.05	1.3	-0.16	0.06							
hek 12									-0.29	0.1	-0.17	0.05	1.4	-0.12	0.06	0.29	0.4	0.53	0.13	0.08		
hek 5									-0.32	0.12	-0.19	0.11	1.3	-0.18	0.06	0.26	0.37	0.52	0	0.08		
hek 14									-0.26	0.06	-0.16	0.05	2.4	-0.15	0.06	0.23	0.37	0.47				
hek 17									-0.25	0.18	-0.16	0.04	2.6	-0.11	0.06	0.26	0.39	0.5				
hek 16									-0.27	0.07	-0.12	0.05	2.6	-0.15	0.06	0.28	0.4	0.56				
hek 21									-0.29	0.15	-0.12	0.07	2.7	-0.17	0.06	0.28	0.4	0.56				
hek 15									-0.22	0.03	-0.13	0.03	3.2	-0.12	0.06	0.32	0.45	0.62				
Anatahan																						
AN-10			18.797		15.566		38.428															
Anat9	0.703		18.790		15.564		38.418															
04-Anat-01			18.779		15.564		38.419															
04-Anat-03	0.703	0.513	18.769		15.563		38.416															
04-Anat-04			18.789		15.559		38.407															
AN-2			18.800		15.568		38.427															
AN-1			18.797	0.004	15.569	0.003	38.440	0.010														
AN-8			18.824	0.001	15.566	0.001	38.412	0.003														
Anat4-s			18.823	0.001	15.566	0.001	38.402	0.003														
AN-12D			18.755	0.001	15.551	0.001	38.335	0.003														
AN-7			18.823	0.001	15.566	0.001	38.402	0.003														
Anat-26-01			18.767	0.001	15.553	0.001	38.341	0.003														
Anat-26-02			18.860	0.002	15.577	0.002	38.506	0.006														
Mariana Central Island Province																						
ALAM 2													1.277	0.082	0.021							
AGR 8B													0.595	-0.113	0.014						-1.1	0.5
PAG 1																					-1.5	0.5
PAG 3																					-0.4	0.5
GUG 4																					-1.2	0.5
GUG 9													0.776	0.067	0.020						-1.1	0.5
MM-92-6													0.998	-0.083	0.022						-1.2	0.5

C. ISOTOPIC DATA

	$^{87}Sr/^{86}Sr$	$^{143}Nd/^{144}Nd$	$^{206}Pb/^{204}Pb$	2sd	$^{207}Pb/^{204}Pb$	2sd	$^{208}Pb/^{204}Pb$	2sd	$d^{30}Si$	2sd	$d^{29}Si$	2sd	Mo	$d^{98}Mo$	2se	$d^{66}Zn$	$d^{67}Zn$	$d^{68}Zn$	$d^{65}Cu$	2sd	$e^{205}Tl$	2sd
GUG3																					-0.5	0.5
GUG11													1.003	0.049	0.016						-1.2	0.5
ALAM5													1.072	0.047	0.014						-0.6	0.5
URA6																					-1.7	0.5
SAG1																					-0.6	0.5
GUG13													0.856	0.038	0.031						1.2	0.5
GUG12													0.894	0.021	0.025						-0.8	0.5
URA5													0.710	0.059	0.015						-1.8	0.5
URA7													0.907	0.054	0.017						-1.1	0.5
URA12													0.909	0.043	0.022						-1.7	0.5
AGR1																						
AGR2													0.492	-0.092	0.018						-1.2	0.5

References

Hekla

Major elements: Savage *et al.*, 2011
Trace elements: Prytulak *et al.*, 2016
Si isotopes: Savage *et al.*, 2011
Mo isotopes: Yang *et al.*, 2015
Zn isotopes: Chen *et al.*, 2013
Cu isotopes: Savage *et al.*, 2015

Anatahan

Major, trace elements: Wade *et al.*, 2005
Radiogenic isotopes: Woodhead, 1989; Woodhead et Fraser, 1985

Mariana Central Island Province

Major elements: Elliott *et al.*, 1997
Trace elements: Elliott *et al.*, 1997 & Prytulak *et al.*, 2013
Mo isotopes: Freymuth *et al.*, 2015
Pb isotopes: Freymuth *et al.*, 2015
Tl isotopes: Prytulak *et al.*, 2013

Table S-2 Vanadium isotopic data.

Sample	$\delta^{51}V$	2sd	number dissolutions	number of measurements	number of sessions	Oxford or Imperial College
Marianas Central Island Province						
SAG1	-0.80	0.14	1	5	2	OX
GUG13	-0.98	0.17	2	8	2	OX
GUG12	-0.84	0.13	1	5	1	OX
URA5	-0.75	0.15	3	8	2	OX
URA7	-0.63	0.21	2	7	2	OX
URA12	-0.77	0.13	2	11	2	OX
AGR1	-0.83	0.09	1	9	3	OX
AGR2	-0.91	0.15	2	21	4	OX
AGR8b	-0.84	0.05	2	8	2	OX
MM-92-6	-0.60	0.08	2	7	2	OX
GUG3	-0.81	0.11	1	3	1	OX
GUG4	-0.73	0.14	1	4	1	OX
GUG11	-0.71	0.17	3	11	2	OX
PAG1	-0.90	0.11	1	4	2	OX
PAG3	-0.85	0.07	2	12	2	OX
ALAM2	-0.81	0.06	2	6	3	OX and IC
ALAM5	-0.83	0.11	1	4	1	OX
URA6	-0.45	0.31	4	11	5	OX
GUG9	-0.85	0.07	1	6	2	OX
Anatahan, Marianas						
04 ANAT 4	-0.95	0.18	1	3	1	IC
04 ANAT 03	-0.26	0.21	2	8	3	IC
ANAT 26-01	-0.59	0.23	1	2	1	IC
04 ANAT 1	0.35	0.33	1	5	2	IC
ANAT 26-02	-0.72	0.14	1	4	2	IC
ANAT 4 as	-0.76	0.15	1	9	2	IC
AN2	-0.39	0.18	2	6	2	IC
AN7	-0.77	0.11	1	4	1	IC
AN12D	0.44	0.39	2	2	1	IC
Anat9	0.97	0.12	1	2	2	IC
AN10	0.55	0.30	2	4	2	IC
AN1	-0.69	0.15	2	9	2	IC
AN8	-0.56	0.08	1	5	1	IC
Hekla, Iceland						
HEK05	-0.65	0.20	2	16	2	OX
HEK06	-0.81	0.01	1	2	1	OX
HEK12	-0.64	0.13	1	11	3	OX
HEK14	0.24	0.08	1	5	2	OX
HEK15	0.92	0.07	1	2	1	OX
HEK16	0.50	0.04	1	5	1	OX
HEK17	0.41	0.11	1	4	1	OX
HEK21	0.46	0.12	1	5	2	OX
USGS Standards (from Prytulak *et al.*, 2011 as lavas data are contemporaneous)						
BIR1a	-0.92	0.16	12	50	8	OX
BHVO1	-0.92	0.04	1	4	1	OX
BHVO2	-0.88	0.10	7	14	4	OX
BCR2	-0.92	0.16	13	27	7	OX
AGV2	-0.58	0.10	4	6	4	OX and IC
GSP2	-0.63	0.10	3	6	1	OX
PCC1	-1.01	0.09	2	8	3	OX
DTS	-0.95	na	1	1	1	OX

Letter Geochemical Perspectives Letters

Table S-3 Fractional crystallisation models.

Anatahan

	Global Input Variables			
	D_V	D_{MgO}	D_{FeO}	$\Delta^{51}V_{min\text{-}melt}$
Plagioclase	0	0	0	0
Magnetite	32	0	6,5	$-0.85*10^6/T^2$
OPX	1,5	6,75	3	$-0.85*10^6/T^2$
CPX	2,5	3,75	1,8	$-0.85*10^6/T^2$

	Modes				Bulk D				Model Output				
F	Plagioclase	Magnetite	OPX	CPX	D_V	D_{MgO}	D_{FeO}	$\Delta^{51}V_{min\text{-}melt}$	V	$\delta^{51}V$	MgO	FeO	T (°C)
1									275	-0.75	5	9	1100
0.95	0.6		0.2	0.2	0.81	2.13	0.99	-0.31	277.8	-0.74	4.7	9	1094.4
0.9	0.6		0.2	0.2	0.81	2.13	0.99	-0.31	280.7	-0.72	4.4	9	1088.8
0.85	0.6		0.2	0.2	0.81	2.13	0.99	-0.31	283.8	-0.71	4.2	9	1083.2
0.8	0.6		0.2	0.2	0.81	2.13	0.99	-0.31	287.2	-0.69	3.9	9	1077.7
0.75	0.6		0.2	0.2	0.81	2.13	0.99	-0.31	290.8	-0.68	3.6	9	1072.2
0.7	0.6	0.01	0.2	0.2	1	2.13	1.03	-0.35	275.2	-0.63	3.3	8.9	1066.8
0.65	0.6	0.01	0.2	0.2	1.13	2.13	1.06	-0.36	260.5	-0.57	3.1	8.8	1061.4
0.6	0.6	0.02	0.19	0.19	1.26	2.05	1.05	-0.38	241.3	-0.5	2.9	8.8	1058.4
0.55	0.6	0.02	0.19	0.19	1.41	2.03	1.07	-0.4	215.7	-0.42	2.7	8.6	1054.2
0.5	0.6	0.03	0.19	0.19	1.56	2	1.09	-0.41	187.1	-0.31	2.5	8.4	1050
0.45	0.6	0.03	0.19	0.19	1.71	1.97	1.11	-0.42	156.5	-0.18	2.3	8.2	1045.9
0.4	0.6	0.04	0.18	0.18	1.86	1.95	1.13	-0.42	125.5	-0.03	2.1	8	1042
0.35	0.6	0.04	0.18	0.18	2.01	1.92	1.15	-0.43	95.6	0.16	1.9	7.7	1038
0.3	0.6	0.05	0.18	0.18	2.16	1.9	1.17	-0.44	68.4	0.38	1.7	7.3	1034
0.25	0.6	0.05	0.18	0.18	2.31	1.87	1.2	-0.44	45	0.66	1.5	6.9	1029.9
0.2	0.6	0.06	0.17	0.17	2.46	1.84	1.22	-0.45	26.4	1.01	1.3	6.4	1025.7
0.15	0.6	0.06	0.17	0.17	2.61	1.82	1.24	-0.45	13.1	1.47	1.1	5.8	1021.2
0.1	0.6	0.07	0.17	0.17	2.76	1.79	1.26	-0.45	4.8	2.13	0.8	5	1016.1
0.05	0.6	0.07	0.17	0.17	2.91	1.77	1.28	-0.46	0.9	3.22	0.5	3.9	1010.1

Geochem. Persp. Let. (2017) 3, 75-84 | doi: 10.7185/geochemlet.1708 SI-18

Letter Geochemical Perspectives Letters

Hekla

	Global Input Variables			
	D_V	D_{MgO}	D_{FeO}	$\Delta^{51}V_{min\text{-}melt}$
Plagioclase	0	0	0	0
Magnetite	42	0	8	$-0.75*10^6/T^2$
OPX	1,5	7,25	3	$-0.75*10^6/T^2$
CPX	2,5	4	1,8	$-0.75*10^6/T^2$

	Modes				Bulk D				Model Output				
F	Plagioclase	Magnetite	OPX	CPX	D_V	D_{MgO}	D_{FeO}	$\Delta^{51}V_{min\text{-}melt}$	V	$\delta^{51}V$	MgO	FeO	T (°C)
1									375	-0.75	5.5	15.75	1110
0.95	0.6	0.06	0.17	0.17	3.24	1.95	1.33	-0.39	334.4	-0.69	5.2	15.5	1104.8
0.9	0.6	0.06	0.17	0.17	3.24	1.95	1.33	-0.39	296.1	-0.62	5	15.2	1099.6
0.85	0.6	0.06	0.17	0.17	3.25	1.95	1.33	-0.39	259.9	-0.55	4.7	14.9	1094.3
0.8	0.6	0.06	0.17	0.17	3.27	1.95	1.33	-0.39	225.9	-0.47	4.5	14.6	1089.1
0.75	0.6	0.06	0.17	0.17	3.29	1.95	1.34	-0.39	193.8	-0.38	4.2	14.3	1083.8
0.7	0.6	0.06	0.17	0.17	3.32	1.95	1.34	-0.39	163.9	-0.29	3.9	13.9	1078.5
0.65	0.6	0.06	0.17	0.17	3.35	1.95	1.35	-0.39	136.3	-0.19	3.7	13.6	1073.2
0.6	0.6	0.06	0.17	0.17	3.38	1.95	1.35	-0.39	111.1	-0.08	3.4	13.1	1067.9
0.55	0.6	0.06	0.17	0.17	3.42	1.95	1.36	-0.39	88.4	0.04	3.1	12.7	1062.5
0.5	0.6	0.07	0.17	0.17	3.45	1.95	1.37	-0.39	68.4	0.18	2.9	12.2	1057.1
0.45	0.6	0.07	0.17	0.17	3.49	1.95	1.37	-0.39	51.2	0.33	2.6	11.7	1051.7
0.4	0.6	0.07	0.17	0.17	3.53	1.95	1.38	-0.39	36.8	0.51	2.3	11.1	1046.2
0.35	0.6	0.07	0.17	0.17	3.57	1.95	1.39	-0.39	25.2	0.71	2	10.5	1040.8
0.3	0.6	0.07	0.17	0.17	3.62	1.95	1.4	-0.39	16.1	0.95	1.8	9.8	1035.2
0.25	0.6	0.07	0.17	0.17	3.66	1.95	1.41	-0.39	9.4	1.23	1.5	9	1029.6
0.2	0.6	0.07	0.17	0.17	3.7	1.95	1.41	-0.39	4.9	1.57	1.2	8.1	1024
0.15	0.6	0.07	0.17	0.17	3.74	1.95	1.42	-0.39	2.1	2.02	0.9	7.1	1018.3
0.1	0.6	0.07	0.17	0.17	3.78	1.95	1.43	-0.39	0.6	2.66	0.6	5.9	1012.5
0.05	0.6	0.07	0.17	0.17	3.83	1.95	1.44	-0.39	0.1	3.74	0.3	4.3	1006.5

Geochem. Persp. Let. (2017) 3, 75-84 | doi: 10.7185/geochemlet.1708 SI-20

Letter Geochemical Perspectives Letters

Table S-4 Example results for non-modal incremental batch melting. Using melting reaction of 0.89cpx + 0.13opx + 0.12sp = 0.13ol + liquid. Partition coefficients from Mallmann and O'Neill (2009).

"MORB"				"ARC"		
FMQ +0.3	V	Sc		FMQ +1.3	V	Sc
D olvine (V8)	0.065	0.284		D olivine	0.021	0.228
D cpx (V1)	0.418	1.440		D cpx (V1)	0.172	1.493
D opx	0.196	0.339		D opx (V5)	0.093	0.339
D spinel	1.552	0.043		D spinel	0.494	0.040

"MORB"										
	Modes 'MORB' source				Bulk Partition Coefficients					
Total Melt F	olivine	opx	cpx	spinel	V	Sc		Cl (V)	Cs (V)	Cl (Sc)	Cs (Sc)
0									79.00		16.30
0.01	0.600	0.200	0.150	0.050	0.218	0.456		354.99	77.77	35.96	15.98
0.02	0.608	0.197	0.137	0.049	0.212	0.438		359.99	76.49	36.70	15.64
0.03	0.616	0.195	0.124	0.049	0.206	0.422		364.18	75.17	37.31	15.30
0.04	0.624	0.192	0.113	0.048	0.200	0.408		367.54	73.81	37.80	14.94
0.05	0.632	0.190	0.103	0.048	0.195	0.394		370.09	72.42	38.16	14.58
0.06	0.640	0.187	0.094	0.047	0.190	0.383		371.85	71.00	38.40	14.21
0.07	0.648	0.185	0.086	0.047	0.186	0.372		372.82	69.55	38.50	13.84
0.08	0.657	0.182	0.078	0.046	0.182	0.363		373.04	68.09	38.48	13.47
0.09	0.665	0.180	0.071	0.045	0.179	0.354		372.53	66.61	38.34	13.09
0.1	0.674	0.178	0.065	0.045	0.175	0.347		371.34	65.12	38.08	12.72
0.11	0.683	0.175	0.059	0.044	0.172	0.340		369.49	63.63	37.72	12.35
0.12	0.692	0.173	0.054	0.044	0.169	0.334		367.03	62.13	37.26	11.98
0.13	0.701	0.171	0.049	0.043	0.166	0.329		364.00	60.63	36.71	11.61
0.14	0.710	0.169	0.045	0.043	0.164	0.325		360.45	59.13	36.09	11.25
0.15	0.719	0.167	0.041	0.042	0.162	0.321		356.41	57.64	35.39	10.90
0.16	0.728	0.164	0.037	0.042	0.160	0.318		351.94	56.17	34.64	10.55
0.17	0.738	0.162	0.034	0.041	0.158	0.315		347.06	54.70	33.83	10.21
0.18	0.747	0.160	0.031	0.041	0.156	0.312		341.83	53.25	32.98	9.87
0.19	0.757	0.158	0.028	0.040	0.154	0.310		336.29	51.81	32.11	9.55
0.2	0.767	0.156	0.026	0.040	0.153	0.309		330.47	50.39	31.20	9.23

Geochem. Persp. Let. (2017) 3, 75-84 | doi: 10.7185/geochemlet.1708 SI-22

Letter Geochemical Perspectives Letters

"ARC"											
		Modes 'ARC' source			Bulk Partition Coefficients						
Total Melt F	olivine	opx	cpx	spinel	V	Sc		Cl (V)	Cs (V)	Cl (Sc)	Cs (Sc)
0									50.00		13.50
0.01	0.650	0.250	0.050	0.050	0.071	0.310		668.56	46.40	42.96	13.06
0.02	0.651	0.247	0.046	0.049	0.069	0.302		631.80	42.99	42.57	12.61
0.03	0.659	0.244	0.041	0.049	0.068	0.297		594.26	39.76	41.83	12.17
0.04	0.668	0.240	0.038	0.048	0.067	0.293		557.69	36.73	41.02	11.74
0.05	0.677	0.237	0.034	0.048	0.066	0.288		522.24	33.88	40.12	11.32
0.06	0.685	0.234	0.031	0.047	0.065	0.285		488.03	31.21	39.16	10.90
0.07	0.694	0.231	0.029	0.047	0.064	0.282		455.16	28.71	38.15	10.50
0.08	0.703	0.228	0.026	0.046	0.064	0.279		423.69	26.38	37.09	10.11
0.09	0.712	0.225	0.024	0.045	0.063	0.276		393.69	24.21	36.00	9.72
0.1	0.722	0.222	0.022	0.045	0.062	0.274		365.17	22.20	34.89	9.35
0.11	0.731	0.219	0.020	0.044	0.061	0.273		338.15	20.33	33.76	8.99
0.12	0.741	0.216	0.018	0.044	0.061	0.271		312.62	18.59	32.63	8.64
0.13	0.750	0.214	0.016	0.043	0.060	0.270		288.58	16.99	31.49	8.30
0.14	0.760	0.211	0.015	0.043	0.060	0.269		266.00	15.51	30.36	7.98
0.15	0.770	0.208	0.014	0.042	0.059	0.268		244.84	14.15	29.24	7.66
0.16	0.780	0.205	0.012	0.042	0.059	0.268		225.06	12.89	28.14	7.36
0.17	0.790	0.203	0.011	0.041	0.058	0.268		206.61	11.73	27.06	7.07
0.18	0.800	0.200	0.010	0.041	0.058	0.268		189.43	10.67	25.99	6.79
0.19	0.811	0.198	0.009	0.040	0.057	0.268		173.48	9.70	24.96	6.52
0.2	0.821	0.195	0.009	0.040	0.057	0.268		158.69	8.81	23.95	6.26

Cl concentration in liquid
Cs concentration in residue

Geochem. Persp. Let. (2017) 3, 75-84 | doi: 10.7185/geochemlet.1708 SI-24

Supplementary Information References

Chen, H., Savage, P.S., Teng, F.-Z., Helz, R.T., Moynier, F. (2013) Zinc isotope fractionation during magmatic differentiation and the isotopic composition of the bulk Earth. *Earth and Planetary Science Letters* 369-370, 34-42.

Elliott, T., Plank, T., Zindler, A., White, W.M., Bourdon, B. (1997) Element transport from slab to volcanic front at the Mariana arc. *Journal of Geophysical Research* 102, 14991-15019.

Feig, S.T., Koepke, J., Snow, J.E. (2010) Effect of oxygen fugacity and water on phase equilibria of a hydrous tholeiitic basalt. *Contributions to Mineralogy and Petrology* 160, 551-568.

Freymuth, H., Vils, F., Willbold, M., Taylor, R.N., Elliott, T. (2015) Molybdenum mobility and isotopic fractionation during subduction at the Mariana arc. *Earth and Planetary Science Letters* 432, 176-186.

Kinzler, R.J. (1997) Melting of mantle peridotite at pressures approaching spinel to garnet transition: application to mid-ocean ridge basalt petrogenesis. *Journal of Geophysical Research* 102, 853-874.

Li, Z-W.A., Lee, C.-T.A. (2004) The constancy of upper mantle fO_2 through time inferred from V/Sc ratios in basalts. *Earth and Planetary Science Letters* 228, 483-493.

Mallmann, G., O'Neill, H.St.C. (2009) The crystal/melt partitioning of V during mantle melting as a function of oxygen fugacity compared with some other elements (Al, P, Ca, Sc, Ti, Cr, Fe, Ga, Y, Zr, Nb). *Journal of Petrology* 50, 1765-1794.

Nielsen, S.G., Prytulak, J., Halliday, A.N. (2011) Determination of precise and accurate $^{51}V/^{50}V$ isotope ratios by MC-ICP-MS, part 1: chemical separation of vanadium and mass spectrometric protocols. *Geostandards and Geoanalytical Research* 35, 293-306.

Nielsen, S.G., Owens, J.D., Horner, T.J. (2016) Analysis of high-precision vanadium isotope ratios by medium resolution MC-IC-MS. *Journal of Analytical Atomic Spectrometry* 31, 531-536.

Nisbet, E.G. (1982) The tectonic setting and petrogenesis of komatiites. In: Arndt, N.T., Nisbet, E.G. (Eds.) *Komatiite*. George Allen and Unwin, London, pp. 501-520.

Prytulak, J., Nielsen, S.G., Halliday, A.N. (2011) Determination of precise and accurate $^{51}V/^{50}V$ isotope ratios by multi-collector ICP-MS, part 2: isotopic composition of six reference materials plus the Allende chondrite and verification tests. *Geostandards and Geoanalytical Research* 35, 307-318.

Prytulak, J., Nielsen, S.G., Plank, T., Barker, M., Elliott, T. (2013) Assessing the utility of thallium and thallium isotopes for tracing subduction zone input to the Mariana arc. *Chemical Geology* 345, 139-149.

Prytulak, J., Brett, A., Webb, M., Plank, T., Rehkamper, M., Savage, P.S., Woodhead, J. (2016) Thallium elemental behavior and stable isotope fractionation during magmatic processes. *Chemical Geology*, doi: 10.1016/j.chemgeo.2016.11.007.

Salters, V.J.M., Stracke, A. (2004) Composition of the depleted mantle. *Geochemistry, Geophysics, Geosystems* 5, doi:10.1029/2003GC000597.

Savage, P.S., Georg, R.B., Williams, H.M., Burton, K.W., Halliday, A.N. (2011) Silicon isotope fractionation during magmatic differentiation. *Geochimica et Cosmochimica Acta* 75, 6124-6139.

Savage, P.S., Moynier, F., Chen, H., Shofner, G., Siebert, J., Badro, J., Puchtel, I.S. (2015) Copper isotope evidence for large-scale sulphide fractionation during Earth's differentiation. *Geochemical Perspectives Letters* 1, 53-64.

Shaw, D.M. (1970) Trace element fractionation during anatexis. *Geochimica et Cosmochimica Acta* 34, 237-243.

Sigmarsson, O., Condomines, M., Fourcade, S. (1992) A detailed Th, Sr, and O isotope study of Hekla: differentiation processes in an Icelandic volcano. *Contributions to Mineralogy and Petrology* 112, 20-34.

Toplis, M.J., Corgne, A. (2002) An experimental study of element partitioning between magnetite, clinopyroxene and iron-bearing silicate liquids with particular emphasis on vanadium. *Contributions to Mineralogy and Petrology* 144, 22-37.

Wade, J.A., Plank, T., Stern, R.J., Tollstrup, D.L., Gill, J.B., O'Leary, J.C., Eiler, J.M., Moore, R.B., Woodhead, J.D., Trusdell, F., Fischer, T.P., Hilton, D.R. (2005) The May 2003 eruption of Anatahan volcano, Mariana Islands: geochemical evolution of a silicic island-arc volcano. *Journal of Volcanology and Geothermal Research* 146, 139-170.

Woodhead, J.D. (1989) Geochemistry of the Mariana arc (western Pacific): source composition and processes. *Chemical Geology* 76, 1-24.

Wu, F., Qi, Y., Yu, H., Tian, S., Hou, Z., Huang, F. (2016) Vanadium isotope measurment by MC-ICP-MS. *Chemical Geology*, 421, 17-25.

Yang, J., Siebert, C., Barling, J., Savage, P.S., Liang, Y.-H., Halliday, A.N. (2015) Absence of molybdenum isotope fractionation during magmatic differentiation at Hekla volcano, Iceland. *Geochimica et Cosmochimica Acta* 162, 126-136.